Universal Quantum Tomography With Deep Neural Networks

Nhan T. Luu, Truong Cong Thang

Department of Computer Science and Engineering

The University of Aizu

Aizuwakamatsu, Japan

(ltnhan0902@gmail.com, thang@u-aizu.ac.jp)

Abstract—**Quantum state tomography is a crucial technique for characterizing the state of a quantum system, which is essential for many applications in quantum technologies. In recent years, there has been growing interest in leveraging neural networks to enhance the efficiency and accuracy of quantum state tomography. Still, many of them did not include mixed quantum state, since pure states are arguably less common in practical situations. In this research paper, we present two neural networks based approach for both pure and mixed quantum state tomography: Restricted Feature Based Neural Network and Mixed States Conditional Generative Adversarial Network, evaluate its effectiveness in comparison to existing neural based methods. We demonstrate that our proposed methods can achieve state-of-the-art results in reconstructing mixed quantum states from experimental data. Our work highlights the potential of neural networks in revolutionizing quantum state tomography and facilitating the development of quantum technologies.**

Index Terms—**quantum state tomography, neural network**

I. INTRODUCTION

A promising avenue for both research and technological advancements has been presented thanks to progress in controlling capacity and manipulation of small quantum systems. These systems offer potential applications in various fields such as quantum information processing and computation [1]–[3], quantum chemistry simulations [4]–[6], secure communication [7], [8], among with others notable works [4], [9], [10]. In recent breakthroughs, the successful demonstration of a 53-qubit quantum computer accomplishing a computational task in a fraction of the time expected on a classical supercomputer [11] underscore the remarkable speedup achievable through quantum systems. This acceleration is attributable in part to the exponentially vast state space available for storing and manipulating information in quantum systems [12]–[14]. Nonetheless, while the expansive state space offers opportunities, it also presents challenges in accurately characterizing and describing these systems.

Quantum State Tomography (QST) [15]–[17] aims to ascertain the unknown quantum state by conducting measurements on a finite set of identical copies of the system. If the state is characterized by the density matrix ϱ, residing in a d-dimensional Hilbert space, approximately $O(d/\varepsilon)$ copies are necessary to achieve an estimate of ϱ with an error (measured as total variation distance) less than ε [18]. This underscores the considerable resource demands of QST for large-scale systems.

In a broader context, QST can be viewed as an inverse problem [19], [20]. Consequently, linear inversion [21] is often considered the most straightforward approach. However, it has drawbacks, such as the potential to yield a non-physical state and the inability to analytically determine the mean squared error bound of the estimate. To address these limitations, several alternative QST methods have been developed, including maximum-likelihood estimation (MLE) [22], [23], Bayesian tomography [24], [25], compressed sensing techniques [26], [27], and matrix-product states [28], [29], where MLE remains the most commonly employed approach.

In recent times, machine learning techniques have been employed in QST, showing promising outcomes [30]–[32]. Specifically, generative models [33]–[35], often in the form of restricted Boltzmann machines (RBMs), have emerged as effective Ansätze with minimal parameters to depict a quantum state and understand the probability distribution of anticipated outputs [30], [36], [37]. Additionally, deep neural networks have been utilized in QST, enabling physicists to harness the swift advancements in machine learning methodologies.

In our research, we introduce QST with 2 type of neural networks (NNs) architecture: Restricted Feature Based Neural Network (RFB-Net) and Mixed States Conditional Generative Adversarial Network (MS-CGAN). RFB-Net is a modified QST-NN [38] with modified regression modules that can classify quantum states into specific specific class and pointing out its features of the quantum state within certain constraints, finally using these features and classes to infer the full state of the system. On the other hand, MS-CGAN is an architecture derived from QST conditional-GAN (QST-CGAN) [39], which contain certain modifications from the original work to extend its reconstruction range to include mixed states. This network is improved for a better estimation of the density matrix of the system while extend reconstruction range to multiple type of quantum states. Both of these techniques can accurately construct many types of given simulated measurement and shown great promise in practical intermediate-scale quantum

systems.

II. EXPERIMENTAL DATA

By the assisstance of QuTiP [40], our generated QST dataset include (but not limited to) 10000 Husimi Q measurements of 32-qubit Coherent states, Fock states, Thermal states, Cat states, Num states [41], [42], Binomial states [41], [42] and GKP states [41], [43], [44] (number of samples uniformly distributed between states), along with the original density matrices, labels and generated values based on certain constraints. Using this diverse set of states in our dataset, we are able to extract many types of information and features .

Typically, these states exist within a Hilbert space that has infinite dimensions. However, we can create a limited representation of these states with finite dimensions by setting a threshold on their energy levels, which is why in our experiments a Hilbert-space cutoff of $N_c = 32$ is used for all cases. To prevent artefacts resulting from truncation, the maximum photon number of the states is limited to 16 after the displacements are applied. Different types of quantum optical states used in the research are defined based on the original paper of QST-NN [38], including three well-known basic classes and four states from bosonic codes designed for quantum error correction.

A. Fock state

Eigenstates of the Fock basis:
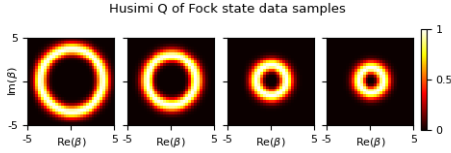
$$|\psi_{fock}\rangle = |n_{photon}\rangle \tag{1}$$

Fig. 1: Samples of Fock state

B. Coherent state

Displaced vacuum states, characterized by the complex displacement amplitude α:

$$|\psi_{coherent}(\alpha)\rangle = |\alpha\rangle = D(\alpha)|0\rangle,$$
$$D(\alpha) = exp(\alpha \times a^\dagger - \alpha \times a) \tag{2}$$

$D(\alpha)$ is the displacement operator where a is the annihilation and $(a^\dagger)$ is the creation operator of the bosonic mode.

C. Thermal state

Mixed states where the photon number distribution follows super-Poissonian statistics:

$$\rho_{thermal}(n^{th}) = \sum_{n=0}^{N_c-1} \frac{1}{n^{th}+1}\left(\frac{n^{th}}{n^{th}+1}\right)^n |n\rangle\langle n| \tag{3}$$
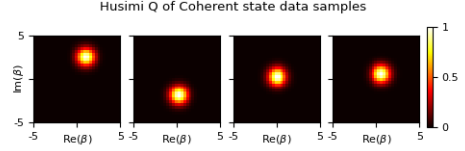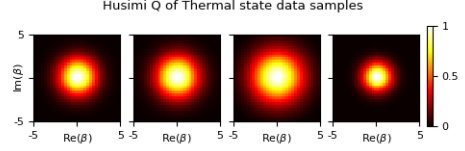

Fig. 2: Samples of Coherent state

Fig. 3: Samples of Thermal state

D. Cat state

Bosonic-code states consisting of superpositions of coherent states up to a normalization N with projections Π_r given by:

$$|\psi_{cat}^\mu\rangle = \frac{1}{N}\Pi_{(S+1)\mu}\left\{\left|\alpha e^{i\frac{\pi}{S+1}k}\right\rangle\right\}_{k=0}^{2S+1},$$
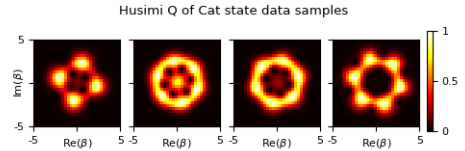$$\Pi_r = \sum_{m=0}^{\infty} |2m(S+1)+r\rangle\langle 2m(S+1)+r| \tag{4}$$

Fig. 4: Samples of Cat state

E. Num state

Specific set of bosonic-code states, consisting of superpositions of a few Fock states, numerically optimized for quantum error correction, and characterized by their average photon number $\overline{n}$
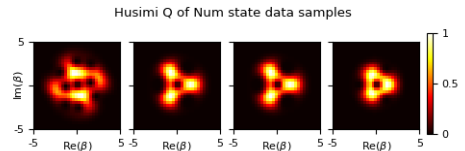

Fig. 5: Samples of Num state

F. Binomial state

Bosonic-code states constructed from a superposition of Fock states weighted by the binomial coefficients:

$$|\psi_{binomial}^{\mu}\rangle = \frac{1}{\sqrt{2^{N+1}}} \sum_{m=0}^{N+1} (-1)^{\mu m} \sqrt{\binom{N+1}{m}} |(S+1)m\rangle \tag{5}$$
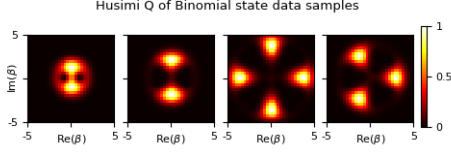

Fig. 6: Samples of Binomial state

G. GKP state

Finite Gottesmann-Kitaev-Preskill states, limits the lattice and adds a Gaussian envelope to make the state normalizable:

$$|\psi_{GKP}^{\mu}\rangle = \sum_{\alpha \in K(\mu)} e^{-\delta^2 |\alpha|^2} e^{-iRe[\alpha]Im[\alpha]} |\alpha\rangle, \\ K(\mu) = \sqrt{\frac{\pi}{2}}(2n_1 + \mu) + i\sqrt{\frac{\pi}{2}}n_2 \tag{6}$$

Fig. 7: Samples of GKP state
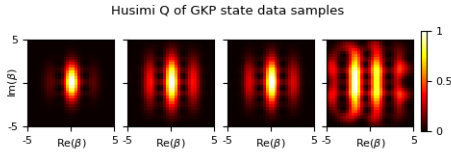
Name	Constraint
Fock state	$1 \le n_{photon} \le 16$
Coherent state	$10^{-6} \le |\alpha|^2 \le 3$
Thermal state	$1 \le n_{th} \le 16$
Cat state	$S \in [0,2], |\alpha| \in [1,3], r \in [0, 2S+1]$
Num state	$\overline{n} \in \{1.56, 2.67, 2.77, 4.15, 4.34\}$
Binomial state	$2 \le N \le N_C/(S+1) - 1$
GKP state	$n_1, n_2 \in \{-20, 20\}, \delta \in [0.2, 0.5]$

TABLE I: Constraints for states in dataset

III. ARCHITECTURE AND TRAINING SETTINGS

A. Restricted Feature Based Neural Network

We utilizes the PyTorch [45] framework to implement a deep convolutional neural network (CNN) similar to QST-NN. In our proposed architecture, we aim to extract relevant information from input measurements that are provided in the form of 32x32 density matrices. To accomplish this, we employ a series of 6 convolutional heads, which are interspersed with Gaussian noise, dropout, and leaky ReLU activation functions to extract meaningful features from the input.

Subsequently, we feed the extracted features into both a classification tail and a regression tail. The classification tail is responsible for predicting the label, while the regression

tail computes three features of the state. To generate the final state prediction, we sum the predicted label output with the extracted features and utilize the regression tail to predict the three essential features of the state.

These three features are then fed into a specialized *Reconstructor* module, which is designed explicitly to reconstruct the state by taking 3-length value vectors as input and generating the predicted states.
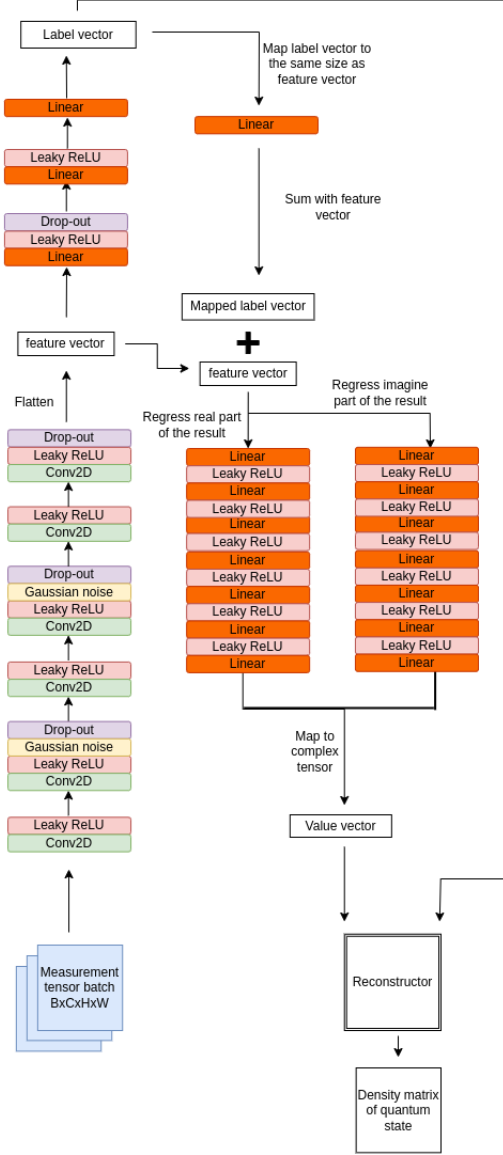

Fig. 8: Architecture of RFB-Net.

We train our model using a linear combination of cross-entropy loss for the label and the sum of MAE loss for the real and imaginary parts of the regression output F as a feature vector:

$$loss = -\sum_{c=1}^{N} label_{real,N} \log(label_{pred,N}) + \\ \sum_{i=1}^{N} \left| F_{out}^{real} - F_{pred}^{real} \right| + \sum_{i=1}^{N} \left| F_{out}^{imag} - F_{pred}^{imag} \right| \qquad (7)$$

In general, the RFB-Net architecture is capable of not only reconstructing states from input measurements but also reconstructing the state from input measurements, which can be viewed as a form of multitasking architecture. In this architecture, the decoder produces both output labels and reconstructed operators. The ability to perform multiple tasks simultaneously is a key feature of multitasking architectures, which are increasingly being used in machine learning applications. By combining multiple tasks into a single architecture, multitasking models can improve efficiency and accuracy, while reducing the computational overhead associated with running separate models for each task. RFB-Net's ability to perform both state reconstruction and label prediction highlights its potential as a versatile and efficient multitasking architecture for quantum information applications. Furthermore, the ability to reconstruct the state from input measurements is particularly useful in quantum information processing, where it is essential to accurately recover the state of a quantum system from measurements. Overall, RFB-Net's multitasking capabilities make it a promising architecture for a wide range of quantum information tasks.

B. Mixed State Conditional Generative Adversarial Network

Building upon the seminal work of QST-CGAN, we have developed a novel neural architecture for state prediction, utilizing the powerful and versatile TensorFlow [46] framework. Our proposed model is designed to accommodate a batch of measurements in the form of 32x32 density matrices, as well as label vectors representing the target state. To facilitate efficient processing, we have implemented a series of pre-processing steps, which include flattening the measurements to a 1024-length vector and one-hot encoding the label to a 7-length vector.

Subsequently, we feed the label vector through a dense layer, which enables us to encode it into a 1024-length vector that can be mapped to the same size as the measurements. By adding the resulting vector and the flattened measurements, we generate a final feature that captures the essence of the underlying quantum state. This final feature is then fed through a series of convolutional layers, batch normalization, and leaky ReLU activation, resulting in a batch of 2x32x32 tensor, where the two channels correspond to the real and imaginary components of the quantum state.

Following the generation of the complex tensor batch, we proceed to further process the data by passing it through a *DensityMatrix* layer, which is responsible for normalizing the quantum state in accordance with specific constraints. Subsequently, we pass the normalized state through an *Expectation* layer, which is designed to measure the state by calculating the expected values of various observables.
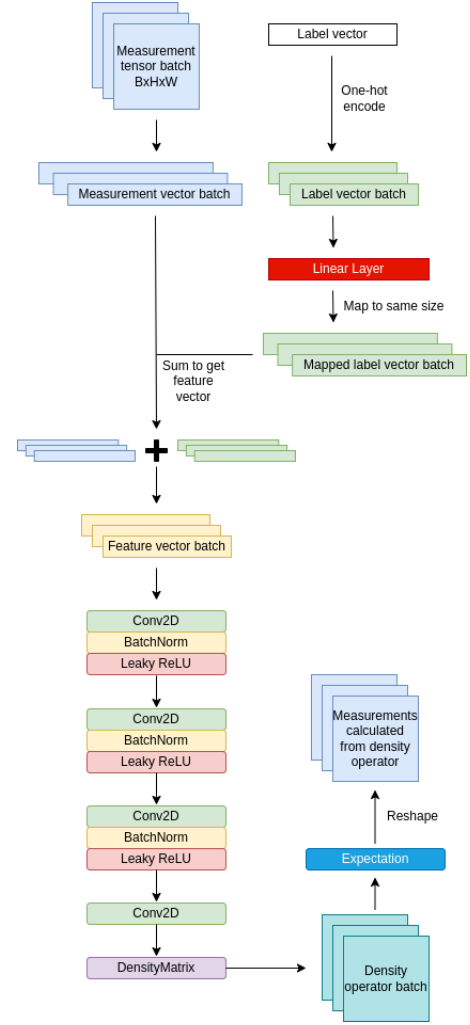

Fig. 9: Architecture of MS-CGAN.

Unlike the original architecture, which only utilizes the lower half of the result to obtain a Hermitian matrix, our novel approach simulate a Cholesky decomposition [22] to the upper half of the result, thereby optimizing the number of parameters utilized in the process. By subtracting the two obtained matrices and normalizing the result, we are able to generate a density operator that encompasses positive semidefinite, negative semi-definite, and even indefinite outcomes.

This approach is particularly relevant in situations where the creation of an odd cat state is required, and can be achieved through the subtraction of two coherent states $|\alpha\rangle$ and $|-\alpha\rangle$:

$$|\psi_{cat}^{\mu}\rangle = \frac{1}{\sqrt{2(1 - e^{-2|\alpha|^2})}}(|\alpha\rangle - |-\alpha\rangle) \qquad (8)$$

Model's loss function is a linear combination of MAE loss of input measurement M_{in} and the measurement from created density matrix M_{pred} with the weighted sum (with a scalar
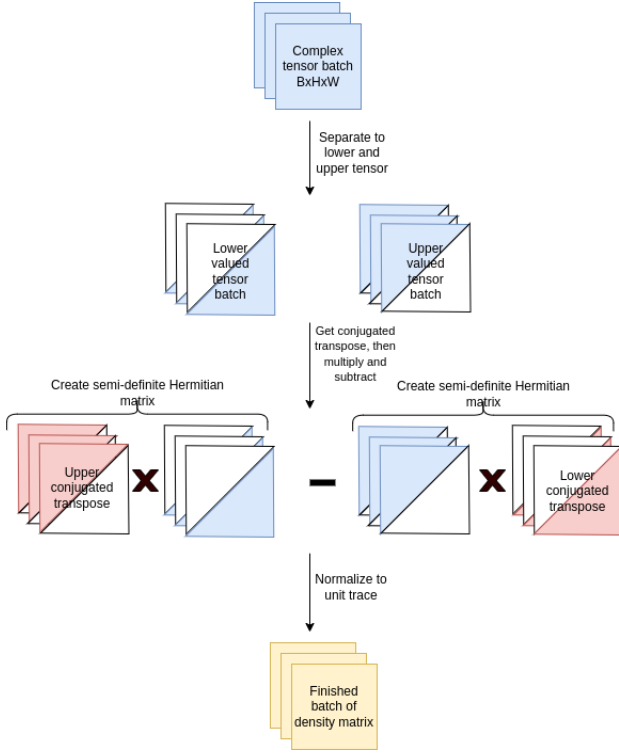
Fig. 10: Demonstration of the improved *DensityMatrix* process.

$\alpha = 100$) of MAE loss for the real and imaginary parts (D^{real} and D^{imag}) of the density operator:

$$
\begin{aligned}
loss = &\sum_{i=1}^{N} |M_{in} - M_{pred}| + \\
&\alpha \times (\sum_{i=1}^{N} \left| D_{true}^{real} - D_{pred}^{real} \right| + \\
&\sum_{i=1}^{N} \left| D_{true}^{imag} - D_{pred}^{imag} \right|)
\end{aligned}
\tag{9}
$$

The model is optimized for 100 epochs on dataset using Adam [47] with $lr = 1e-4$ and $\beta = (0.9, 0.999)$. Our experimental results show that our proposed architecture has the potential to cover every quantum state that can be represented as a density operator, which is a Hermitian matrix with unit trace. This makes our architecture a more optimized solution for state prediction problems in various applications, as it can handle a wider range of quantum states.

C. Accuracy metrics

In both of our experiment, we will be using quantum fidelity to measure the similarity between two quantum states. Quantum fidelity is a key concept in quantum information theory and plays a critical role in many quantum information protocols, including quantum error correction, quantum teleportation, and quantum cryptography. Given two density matrices ρ and σ, the fidelity is defined by :

$$
F(\rho, \sigma) = (tr(\sqrt{\sqrt{\rho}\sigma}))^2
\tag{10}
$$

where if $F(\rho, \sigma) == 1$, the two states are identical. If the fidelity is $0 \leq F(\rho, \sigma) < 1$, the two states differ, and the degree of difference is quantified by the fidelity value.

IV. RESULT

Within this section, we shall expound upon the findings of our investigation, in which we leveraged two distinct neural network architectures for quantum tomography. Our analysis of these models yielded remarkable outcomes, as both demonstrated adequate performance in reconstructing the states of quantum systems.

The experimentation of both models are conducted on a single NVIDIA GeForce RTX 3080 GPU.

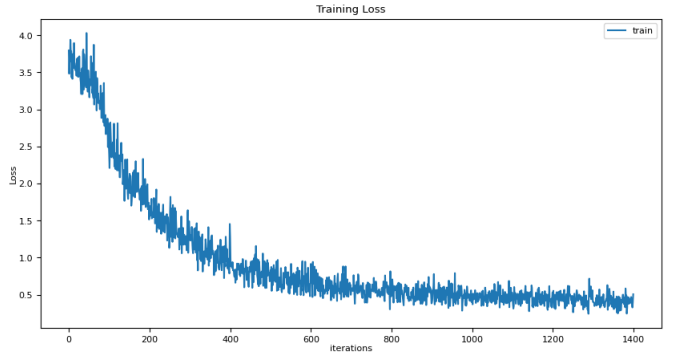### A. Restricted Feature Based Neural Network
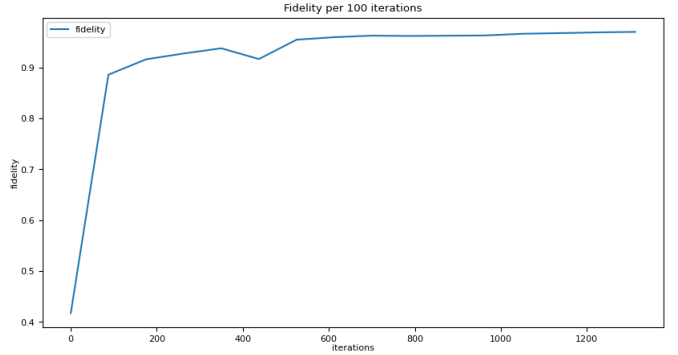

Fig. 11: Training loss progression of RFB-Net.

Fig. 12: Validation fidelity progression per 100 iterations of RFB-Net.

RFB-Net were initially trained for 100 epochs using Adam [47] optimizer with $lr = 1e-4$ and $\beta = (0.9, 0.999)$. Although the model have already converge majorly post training with this setting, we want to explore how long would it take for the model to completely converge close to state of the art result. After throughout examining, we see that it took at least around 1000 epochs for model to converge close to state of the art result.

Figure 12 demonstrate that the model's degree of fidelity converges to a noteworthy value within the initial 100 epochs. However, to achieve an even higher degree of fidelity, it is necessary to engage in a protracted training process of over 1300 epochs, which can be considerably time-consuming. The probable cause behind this gradual convergence is due to the model's need for a more extensive fine-tuning process, which would enable it to make accurate predictions of vectors that contain small values, such as when predicting the mean photon number of a coherent state. This implies that the model's ability to make precise predictions is contingent on the length of the fine-tuning process, and a lengthier process would enable the model to offer better predictions.

To attain fidelity of the proposed architecture, the deployment of the *Reconstruction* module is imperative to restore the state from the predicted values. Given the significant computational expense incurred during the process of reconstruction, a judicious decision was made to evaluate the architecture's fidelity after every 100 epochs. This approach allows for a systematic assessment of the performance of the architecture, while minimizing the computational burden of reconstructing the state at every epoch.

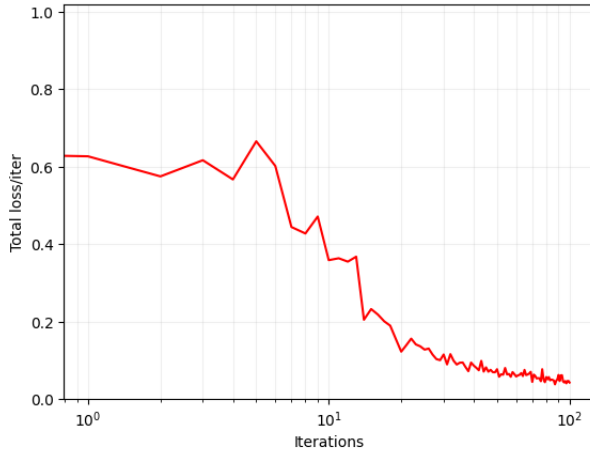### B. Mixed State Conditional Generative Adversarial Network

Fig. 13: Training loss progression of MS-CGAN.

The MS-CGAN architecture exhibits a distinct characteristic when compared to the RFB-Net architecture, in that it is capable of converging to desired values within a training period consisting of no more than 100 iterations (Figure 13 and 14), despite requiring an extra label input in comparison to the RFB-Net architecture. Notably, the MS-CGAN architecture is primarily focused on reconstruction, but this does not detract from its robustness, given its swift convergence when trained on relevant data. It is therefore reasonable to conclude that the MS-CGAN architecture is a viable alternative to the RFB-Net architecture, given its impressive performance characteristics in terms of convergence speed and accuracy, despite having

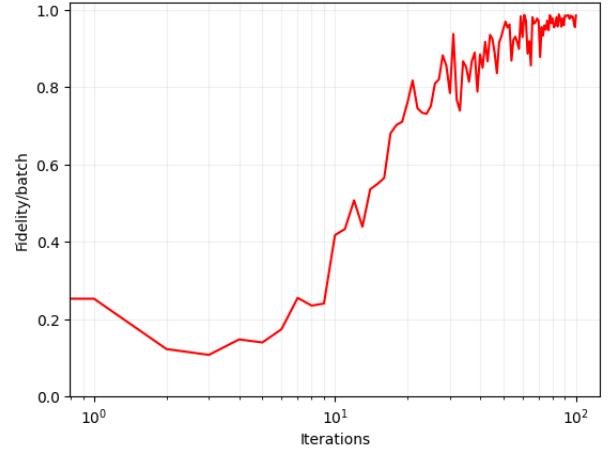
Fig. 14: Validation fidelity progession of MS-CGAN during training process.

distinct differences in terms of input requirements and model focus.

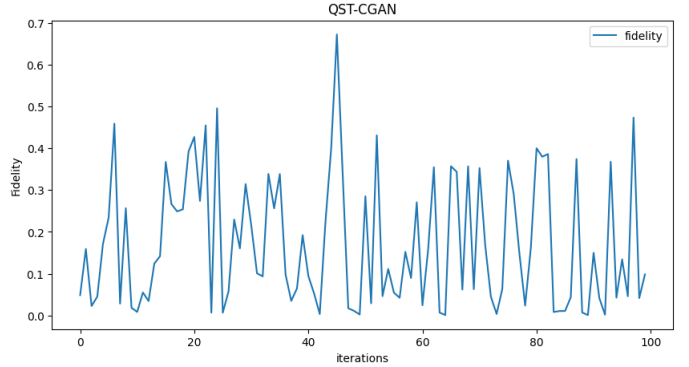### C. Compare with existing methods

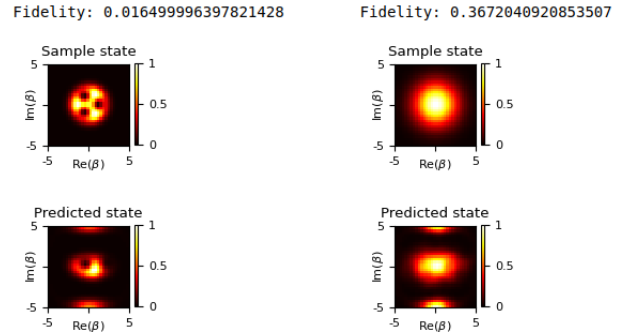Fig. 15: Validation fidelity progression of QST-CGAN on generated dataset.

Fig. 16: Samples of QST-CGAN predictions.

Model name	Fidelity
RFB-Net	0.97
MS-CGAN	0.91
QST-CGAN	0.19

TABLE II: Validation fidelity of investigated models on generated dataset.

In order to ensure a more robust and comprehensive comparison between our proposed model and the original model, we have undertaken a meticulous and rigorous experimental procedure that involves the use of a QST-CGAN model trained on the same dataset for a prolonged period of 100 epochs, utilizing the original configuration parameters and settings as described in the seminal paper. This approach is intended to provide a more nuanced and detailed analysis of the comparative performance of the two models, by subjecting both models to identical experimental conditions, and enabling us to assess their relative strengths and weaknesses in a more systematic and rigorous manner.

Upon conducting this extensive analysis, we have observed that the QST-CGAN model, while exhibiting notable strengths and advantages in certain areas, has encountered certain challenges and limitations in the reconstruction of specific batches of states, resulting in an unstable and erratic convergence on the dataset. These limitations are reflected in the average fidelity score, which is found to be hovering around a modest 0.19, indicating a suboptimal and unsatisfactory level of accuracy and precision. In contrast, our proposed solution has proven to be more superior and effective in overcoming these challenges, by demonstrating a higher degree of stability, robustness, and accuracy, as well as a more consistent and reliable performance.

D. Benchmarking with noise

The presence of noise, which refers to any unwanted fluctuations or disturbances in the experimental setup, is an inescapable factor that pervades most scientific investigations, and consequently poses significant challenges for accurate and reliable data analysis. Given this ubiquitous nature of noise, it is imperative that any method employed for state reconstruction is designed and optimized to be robust and resilient against various types of noise, to ensure that the final results are valid and trustworthy.

Moreover, it is essential to recognize that noise can infiltrate the system at multiple stages, leading to a potentially complex and nuanced interplay of factors that can affect the experimental outcome. Specifically, noise can manifest itself during the preparation of the state to be reconstructed, where errors in the preparation procedure can introduce small deviations in the actual state of interest, resulting in a distorted or altered version of the target state. Additionally, the measurement protocol itself can be a source of noise, as any calibration errors or other external influences may cause us to measure something
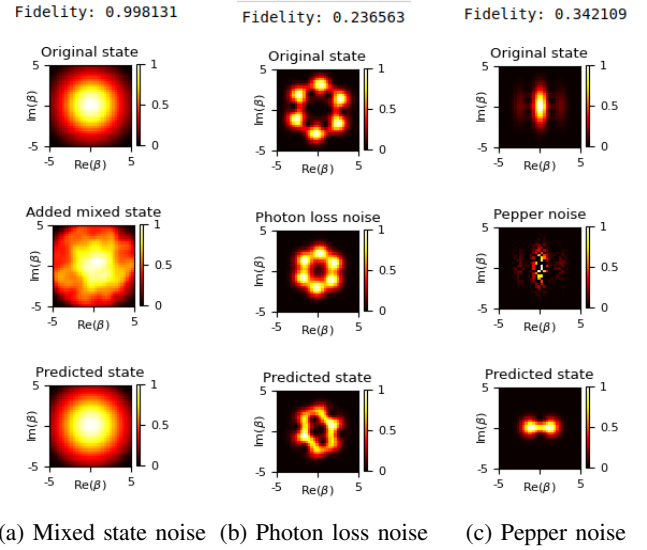

(a) Mixed state noise (b) Photon loss noise (c) Pepper noise

Fig. 17: Samples of noisy input and RFB-Net predictions.

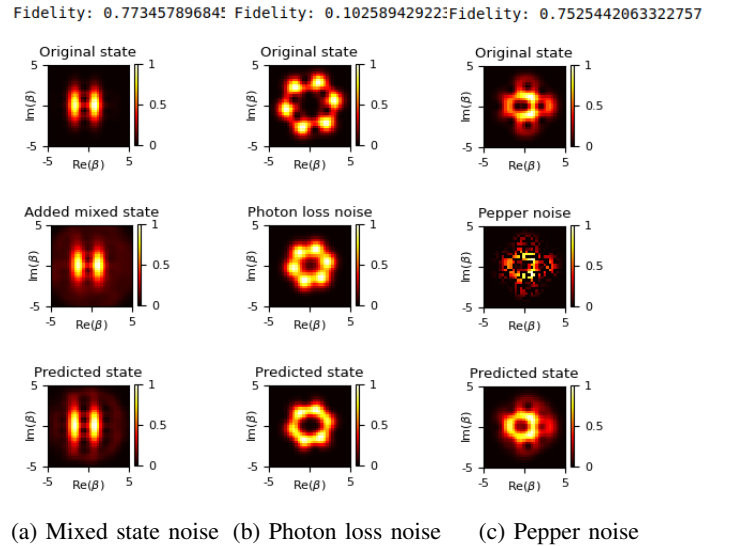(a) Mixed state noise (b) Photon loss noise (c) Pepper noise

Fig. 18: Samples of noisy input and MS-CGAN predictions.

other than what we intended to measure, leading to further inaccuracies in the final results. Finally, noise can arise during the data collection process itself, where amplification errors or photon shot noise can corrupt the signal, leading to further challenges in data interpretation and analysis. Therefore, a comprehensive and multifaceted approach is needed to account for the various sources of noise and ensure that any method for state reconstruction is adequately robust and resilient against these influences, to provide accurate and reliable results that can be used to advance scientific knowledge and understanding.

In this research, our approach involves the utilization of various noise generating techniques, akin to the employed

	Noise type		
Model name	Mixed state noise	Photon loss noise	Pepper noise
RFB-Net	0.80	0.51	0.30
MS-CGAN	0.49	0.48	0.60

TABLE III: Average fidelity of reconstructed noisy data

dataset, taken from QST-NN. In particular, we have employed three types of noise in our experiment, which include additive mixed state noise, photon loss noise, and pepper noise. Rather than introducing the noise during the training phase, whereby the model would gradually learn and adapt to it, we have opted to evaluate the performance of two distinct architectures devoid of exposure to noisy data. This is to ascertain whether our models can generalize well under these conditions or not.

Upon analyzing the sample input and prediction, it is evident that the RFB-Net exhibits a commendable performance in noisy environments in comparison to the MS-CGAN with regards to fidelity, albeit the reconstructed operator showcasing some dissimilarities from its original form. On the other hand, the MS-CGAN's performance is more stable, particularly when dealing with pepper noise added samples, and shows superior feature extraction capabilities compared to RFB-Net.

V. CONCLUSION

In summary, this research paper explored the application of neural networks in quantum tomography, and the findings suggest that they offer a promising approach to solving the challenges associated with reconstructing quantum states. The results demonstrate that neural network architectures, when trained on appropriate datasets, can produce accurate and efficient reconstructions of quantum states. Furthermore, the approach presented in this paper is scalable and can be extended to large-scale quantum systems. It is clear that the combination of neural networks and quantum tomography has great potential for advancing the field of quantum information processing, and we anticipate that this research will inspire further exploration and development of these methods in the future.

REFERENCES

[1] R. P. Feynman, "Simulating physics with computers," in *Feynman and computation*. CRC Press, 2018, pp. 133–153.

[2] A. Montanaro, "Quantum algorithms: an overview," *npj Quantum Information*, vol. 2, no. 1, pp. 1–8, 2016.

[3] G. Wendin, "Quantum information processing with superconducting circuits: a review," *Reports on Progress in Physics*, vol. 80, no. 10, p. 106001, 2017.

[4] I. M. Georgescu, S. Ashhab, and F. Nori, "Quantum simulation," *Reviews of Modern Physics*, vol. 86, no. 1, p. 153, 2014.

[5] A. Kandala, A. Mezzacapo, K. Temme, M. Takita, M. Brink, J. M. Chow, and J. M. Gambetta, "Hardware-efficient variational quantum eigensolver for small molecules and quantum magnets," *nature*, vol. 549, no. 7671, pp. 242–246, 2017.

[6] A. M. Childs, D. Maslov, Y. Nam, N. J. Ross, and Y. Su, "Toward the first quantum simulation with quantum speedup," *Proceedings of the National Academy of Sciences*, vol. 115, no. 38, pp. 9456–9461, 2018.

[7] H. J. Kimble, "The quantum internet," *Nature*, vol. 453, no. 7198, pp. 1023–1030, 2008.

[8] J. Yin, Y.-H. Li, S.-K. Liao, M. Yang, Y. Cao, L. Zhang, J.-G. Ren, W.-Q. Cai, W.-Y. Liu, S.-L. Li *et al.*, "Entanglement-based secure quantum cryptography over 1,120 kilometres," *Nature*, vol. 582, no. 7813, pp. 501–505, 2020.

[9] J.-Q. You and F. Nori, "Atomic physics and quantum optics using superconducting circuits," *Nature*, vol. 474, no. 7353, pp. 589–597, 2011.

[10] X. Gu, A. F. Kockum, A. Miranowicz, Y.-x. Liu, and F. Nori, "Microwave photonics with superconducting quantum circuits," *Physics Reports*, vol. 718, pp. 1–102, 2017.

[11] F. Arute, K. Arya, R. Babbush, D. Bacon, J. C. Bardin, R. Barends, R. Biswas, S. Boixo, F. G. Brandao, D. A. Buell *et al.*, "Quantum supremacy using a programmable superconducting processor," *Nature*, vol. 574, no. 7779, pp. 505–510, 2019.

[12] M. A. Nielsen and I. L. Chuang, *Quantum computation and quantum information*. Cambridge university press, 2010.

[13] C. M. Caves, I. H. Deutsch, and R. Blume-Kohout, "Physical-resource requirements and the power of quantum computation," *Journal of Optics B: Quantum and Semiclassical Optics*, vol. 6, no. 8, p. S801, 2004.

[14] V. Havlíček, A. D. Córcoles, K. Temme, A. W. Harrow, A. Kandala, J. M. Chow, and J. M. Gambetta, "Supervised learning with quantum-enhanced feature spaces," *Nature*, vol. 567, no. 7747, pp. 209–212, 2019.

[15] G. M. D'Ariano, M. G. Paris, and M. F. Sacchi, "Quantum tomography," *Advances in imaging and electron physics*, vol. 128, no. 10.1016, pp. S1076–5670, 2003.

[16] Y.-x. Liu, L. Wei, and F. Nori, "Tomographic measurements on superconducting qubit states," *Physical Review B*, vol. 72, no. 1, p. 014547, 2005.

[17] A. I. Lvovsky and M. G. Raymer, "Continuous-variable optical quantum-state tomography," *Reviews of modern physics*, vol. 81, no. 1, p. 299, 2009.

[18] R. O'Donnell and J. Wright, "Efficient quantum tomography," in *Proceedings of the forty-eighth annual ACM symposium on Theory of Computing*, 2016, pp. 899–912.

[19] A. Tarantola, *Inverse problem theory and methods for model parameter estimation*. SIAM, 2005.

[20] R. C. Aster, B. Borchers, and C. H. Thurber, *Parameter estimation and inverse problems*. Elsevier, 2018.

[21] B. Qi, Z. Hou, L. Li, D. Dong, G. Xiang, and G. Guo, "Quantum state tomography via linear regression estimation," *Scientific reports*, vol. 3, no. 1, p. 3496, 2013.

[22] K. Banaszek, G. D'ariano, M. Paris, and M. Sacchi, "Maximum-likelihood estimation of the density matrix," *Physical Review A*, vol. 61, no. 1, p. 010304, 1999.

[23] A. I. Lvovsky, "Iterative maximum-likelihood reconstruction in quantum homodyne tomography," *Journal of Optics B: Quantum and Semiclassical Optics*, vol. 6, no. 6, p. S556, 2004.

[24] R. Blume-Kohout, "Optimal, reliable estimation of quantum states," *New Journal of Physics*, vol. 12, no. 4, p. 043034, 2010.

[25] C. Granade, J. Combes, and D. Cory, "Practical bayesian tomography," *new Journal of Physics*, vol. 18, no. 3, p. 033024, 2016.

[26] D. Gross, Y.-K. Liu, S. T. Flammia, S. Becker, and J. Eisert, "Quantum state tomography via compressed sensing," *Physical review letters*, vol. 105, no. 15, p. 150401, 2010.

[27] D. Ahn, Y. S. Teo, H. Jeong, F. Bouchard, F. Hufnagel, E. Karimi, D. Koutnỳ, J. Řeháček, Z. Hradil, G. Leuchs *et al.*, "Adaptive compressive tomography with no a priori information," *Physical Review Letters*, vol. 122, no. 10, p. 100404, 2019.

[28] M. Cramer, M. B. Plenio, S. T. Flammia, R. Somma, D. Gross, S. D. Bartlett, O. Landon-Cardinal, D. Poulin, and Y.-K. Liu, "Efficient quantum state tomography," *Nature communications*, vol. 1, no. 1, p. 149, 2010.

[29] B. Lanyon, C. Maier, M. Holzäpfel, T. Baumgratz, C. Hempel, P. Jurcevic, I. Dhand, A. Buyskikh, A. Daley, M. Cramer *et al.*, "Efficient tomography of a quantum many-body system," *Nature Physics*, vol. 13, no. 12, pp. 1158–1162, 2017.

[30] G. Carleo and M. Troyer, "Solving the quantum many-body problem with artificial neural networks," *Science*, vol. 355, no. 6325, pp. 602–606, 2017.

[31] Q. Xu and S. Xu, "Neural network state estimation for full quantum state tomography," *arXiv preprint arXiv:1811.06654*, 2018.

[32] G. Torlai, G. Mazzola, J. Carrasquilla, M. Troyer, R. Melko, and G. Carleo, "Neural-network quantum state tomography," *Nature Physics*, vol. 14, no. 5, pp. 447–450, 2018.

[33] J. Carrasquilla, G. Torlai, R. G. Melko, and L. Aolita, "Reconstructing quantum states with generative models," *Nature Machine Intelligence*, vol. 1, no. 3, pp. 155–161, 2019.

[34] S. Lloyd and C. Weedbrook, "Quantum generative adversarial learning," *Physical review letters*, vol. 121, no. 4, p. 040502, 2018.

[35] M. Kieferová and N. Wiebe, "Tomography and generative training with quantum boltzmann machines," *Physical Review A*, vol. 96, no. 6, p. 062327, 2017.

[36] I. Glasser, N. Pancotti, M. August, I. D. Rodriguez, and J. I. Cirac, "Neural-network quantum states, string-bond states, and chiral topological states," *Physical Review X*, vol. 8, no. 1, p. 011006, 2018.

[37] E. S. Tiunov, V. Tiunova, A. E. Ulanov, A. Lvovsky, and A. K. Fedorov, "Experimental quantum homodyne tomography via machine learning," *Optica*, vol. 7, no. 5, pp. 448–454, 2020.

[38] S. Ahmed, C. Sánchez Muñoz, F. Nori, and A. F. Kockum, "Classification and reconstruction of optical quantum states with deep neural networks," *Physical Review Research*, vol. 3, no. 3, p. 033278, 2021.

[39] S. Ahmed, C. Sanchez Munoz, F. Nori, and A. F. Kockum, "Quantum state tomography with conditional generative adversarial networks," *Physical review letters*, vol. 127, no. 14, p. 140502, 2021.

[40] J. R. Johansson, P. D. Nation, and F. Nori, "Qutip: An open-source python framework for the dynamics of open quantum systems," *Computer Physics Communications*, vol. 183, no. 8, pp. 1760–1772, 2012.

[41] V. V. Albert, K. Noh, K. Duivenvoorden, D. J. Young, R. Brierley, P. Reinhold, C. Vuillot, L. Li, C. Shen, S. M. Girvin *et al.*, "Performance and structure of single-mode bosonic codes," *Physical Review A*, vol. 97, no. 3, p. 032346, 2018.

[42] M. H. Michael, M. Silveri, R. Brierley, V. V. Albert, J. Salmilehto, L. Jiang, and S. M. Girvin, "New class of quantum error-correcting codes for a bosonic mode," *Physical Review X*, vol. 6, no. 3, p. 031006, 2016.

[43] P. Campagne-Ibarcq, A. Eickbusch, S. Touzard, E. Zalys-Geller, N. E. Frattini, V. V. Sivak, P. Reinhold, S. Puri, S. Shankar, R. J. Schoelkopf *et al.*, "Quantum error correction of a qubit encoded in grid states of an oscillator," *Nature*, vol. 584, no. 7821, pp. 368–372, 2020.

[44] D. Gottesman, A. Kitaev, and J. Preskill, "Encoding a qubit in an oscillator," *Physical Review A*, vol. 64, no. 1, p. 012310, 2001.

[45] A. Paszke, S. Gross, F. Massa, A. Lerer, J. Bradbury, G. Chanan, T. Killeen, Z. Lin, N. Gimelshein, L. Antiga *et al.*, "Pytorch: An imperative style, high-performance deep learning library," *Advances in neural information processing systems*, vol. 32, 2019.

[46] M. Abadi, P. Barham, J. Chen, Z. Chen, A. Davis, J. Dean, M. Devin, S. Ghemawat, G. Irving, M. Isard *et al.*, "{TensorFlow}: a system for {Large-Scale} machine learning," in *12th USENIX symposium on operating systems design and implementation (OSDI 16)*, 2016, pp. 265–283.

[47] D. P. Kingma and J. Ba, "Adam: A method for stochastic optimization," *arXiv preprint arXiv:1412.6980*, 2014.